

RSC Advances



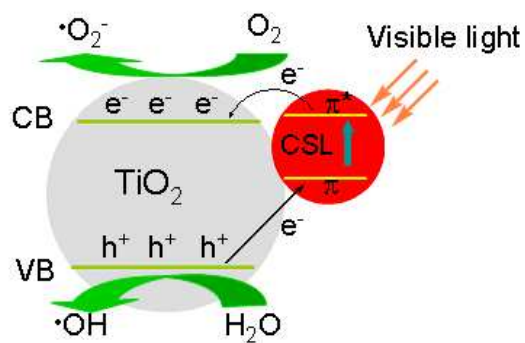
This is an *Accepted Manuscript*, which has been through the Royal Society of Chemistry peer review process and has been accepted for publication.

Accepted Manuscripts are published online shortly after acceptance, before technical editing, formatting and proof reading. Using this free service, authors can make their results available to the community, in citable form, before we publish the edited article. This *Accepted Manuscript* will be replaced by the edited, formatted and paginated article as soon as this is available.

You can find more information about *Accepted Manuscripts* in the [Information for Authors](#).

Please note that technical editing may introduce minor changes to the text and/or graphics, which may alter content. The journal's standard [Terms & Conditions](#) and the [Ethical guidelines](#) still apply. In no event shall the Royal Society of Chemistry be held responsible for any errors or omissions in this *Accepted Manuscript* or any consequences arising from the use of any information it contains.

Table of contents



Celastrol-modified TiO_2 nanoparticles were synthesized by mild hydrothermal method and the modification of CSL exhibit higher visible-light photocatalytic activity.

Celastrol-modified TiO₂ nanoparticles: Effects of celastrol on the particles size and visible-light photocatalytic activity

Caihua Chen^a, Quanwen Liu^{a,*}, Shanmin Gao^{a,b,*}, Kai Li^a, Hui Xu^a, Zaizhu Lou^b, Baibiao

Huang^b and Ying Dai^b

^a College of Chemistry & Materials Science, Ludong University, Yantai, 264025, China.

^b State Key Laboratory of Crystal Materials, Shandong University, Jinan, 250100, China.

Abstract

In this study, celastrol (CSL), a triterpene compound which is derived from the Chinese medicinal plant *Tripterygium wilfordii*, was used to synthesize CSL-modified TiO₂ nanoparticles by hydrothermal treatment method. The nanoparticles phase, morphology, surface structures, as well as the visible-light photocatalytic activities are studied. The modification of CSL does not alter the crystalline structure of the TiO₂ but can prevent TiO₂ from further aggregating and provides photosynthesis pigments as *in situ* dye-sensitizing source. Compared to pure TiO₂, the resulting CSL-modified TiO₂ nanoparticles exhibit enhanced visible-light photocatalytic activity and showed an excellent cyclic stability on the decomposition of methylene blue (MB). In addition, the photocatalytic degradations of MB were all demonstrated to follow first-order kinetic model. The enlarged specific surface area and CSL-modified surface improved the visible-light photocatalytic activity of nanoparticles.

Key words: TiO₂, CSL-modified, nanoparticles, visible-light photocatalytic

1. Introduction

Anatase TiO₂ is an excellent photocatalyst, because it is effective, photostable, reusable, inexpensive and non-toxic.¹ Generally, in the TiO₂-catalyzed photo-oxidation process, the photoexcited electrons in the conduction band (CB) of TiO₂ (-4.2 eV vs vacuum) can be readily captured by O₂ to form superoxide anions (O₂⁻) as well as other oxygen species, while the holes in the valence band (VB, -7.4 eV vs vacuum) resides below the highest occupied molecular orbitals (HOMO) of most organic pollutants, allowing aggressive oxidizing (ripping electrons off) the organic pollutants.² However, because of its large band gap of 3.2 eV, only a small UV fraction of solar light, about 4%, can be utilized to generate electron-hole pairs. To extend the light response of TiO₂ to the visible region, many modification methods, such as metal ion and non-metal doping,³ noble metal deposition,⁴ Ti³⁺ self-doping,⁵ composite semiconductors,⁶ and surface dye sensitization have been reported.^{7,8}

Some studies have showed that surface dye sensitization or modification by conductive polymers can be used to improve its photocatalytic activity by absorbing visible light and subsequently transferring photogenerated electrons from excited sensitizer molecules to the conduction band of TiO₂.⁹⁻¹¹ In addition, it was found that certain organic species could be modified on the surface of TiO₂ and showed higher photocatalytic activity.¹²⁻¹⁴ For example, Yu et al. prepared trifluoroacetic acid (TFA) modified TiO₂ hollow microspheres by one-pot hydrothermal treatment of Ti(SO₄)₂ in the presence of TFA at 180°C for 12 h.¹⁵ Cropek et al. found that surface modification of TiO₂ with arginine changed the surface charge and resulted in enhanced reduction of 4-nitrophenol.¹⁶ Feng et al. investigated the preparation of phthalic acid

modified TiO₂ and found that the adsorption of phthalic acid onto the surface of TiO₂ nanoparticles resulted in the formation of a surface-modified complex. The recombination of charge carriers was effectively suppressed due to the modification of phthalic acid on the surface of TiO₂.¹⁷

Recently, Shi et al. reported that surface-sensitized TiO₂ with quercetin can result in inhibition of *Helminthosporium maydis* under visible light irradiation.¹⁸ Quercetin, a kind of flavonoids extracted from natural plants, on the one hand, has a catechol moiety that can coordinate with surface sites of TiO₂ nanoparticles to form a charge-transfer complex, which can enhance the rate constant of electron transfer from adsorbed species to TiO₂ semiconductor. On the other hand, the dye can act as surface photosensitizer because of the presence of the π -conjugated system in quercetin molecular structure and hyper chromic groups (–OH) on its chromone moiety, making the TiO₂ absorb and respond to visible light.

Celastrol (CSL) is an orange-coloured triterpene compound containing an acidic group on one end and a phenolic quinone at the other end, which is derived from the Chinese medicinal plant *Tripterygium wilfordii*. In China, this plant has a long history of use in traditional medicine for treating fever and joint pain. It has attracted great attention for its potent anti-inflammatory effects, anticancer effects and antioxidation.¹⁹ Evidence has been obtained that the dienone-phenol moiety and the anionic carboxyl group of CSL are both required for efficient antiperoxidative action. The phenol directly scavenges radicals while the latter contributes a negative surface charge to the cell membrane.²⁰ Wang et al. investigated the photodynamic treatment of TiO₂ nanofibers combined with CSL for HepG2 proliferation in vitro.²¹ Their results

indicated that the nanocomposites between TiO₂ nanofibers and CSL could enhance the cytotoxicity of CSL for HepG2 cells and cut down the drug consumption so as to reduce the side-effect of the related drug.

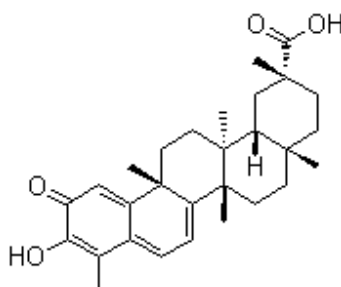
In this paper, the TiO₂ nanoparticles modified by a small amount of CSL were prepared and the visible light photocatalytic activities of it were investigated. To the best of our knowledge, no work has been done on the photocatalytic activity of CSL-modified TiO₂ nanoparticles under visible light irradiation. On the one hand, CSL can affect the size and shape of the TiO₂ nanoparticles. On the other hand, the CSL-modified TiO₂ absorbed more photons under visible light irradiation. A possible mechanism for MB dyes photodegradation by using CSL-modified TiO₂ nanoparticles was also preliminarily discussed. The dramatic enhancement in photocatalytic activity under visible light irradiation was explained on the basis of the synergetic effects of enhanced adsorption of the CSL and improved efficiency on separation of photo-generated carriers.

2. Materials and Method

2.1 Synthesis

The CSL was extract from *Tripterygium wilfordii* by our own. Its structure is given in Scheme 1. Other chemicals used in this study were reagent-grade and deionized water was used in all experiments. A typical procedure for preparing the CSL-modified TiO₂ nanoparticles is described as following. First, 6.0 g tetrabutyl orthotitanate (Ti(OC₄H₉)₄, TBOT) was dissolved in 20 mL absolute ethyl alcohol, and the solution was stirred for 10 min at ambient temperature to

achieve homogeneity. 0.03 g CSL was dissolved in 20 mL absolute ethyl alcohol, and the CSL solution was added drop-wise into the TBOT solution with continuous stirring for 15 min at room temperature. Then, 100 mL distilled water were added to the mixture solution of CSL and TBOT, which leads to a red-brown precipitate of floccules immediately. During hydrolysis, the liquid was kept under continuous vigorous stirring and the resulting suspension was continuously stirred for an additional 1 h at room temperature. The precipitate was filtered out and washed repeatedly with deionized water and absolute ethanol. Then the precipitate was treated at 180°C for 24 h by hydrothermal method. Finally, the precipitate was filtered out and washed by deionized water and absolute ethanol for multiple times and dried in an oven at 80°C for 4 h. For comparison, pure TiO₂ powder was also prepared without the addition of the CSL.



Scheme 1. Structure of celastrol

2.2 Characterization

The phases of the final products were identified using X-ray diffractometer (XRD) (Rigaku D/max-2500VPC) with Ni-filtered Cu K α radiation at a scanning rate of 0.02° s⁻¹ from 20° to 80°. The morphology of the samples was observed with a Hitachi model H800 transmission electron microscope (TEM) using an accelerating voltage of 150 kV. Ultraviolet–visible (UV-vis) diffuse reflection spectra (DRS) were recorded on a Shimadzu UV-2550 UV-vis

spectrophotometer in the range 200–800 nm at room temperature. Fourier transform infrared (FT-IR) spectra were recorded from KBr pellets in a Nicolet Nexus 670 spectrophotometer. The photoluminescence (PL) spectra were measured at room temperature with a Perkin Elmer LS 55 Fluorescence Spectrometer, using pulsed Xenon discharge lamps as excitation sources.

2.3 Photocatalytic Measurement

The photocatalytic activity of the as-prepared CSL-modified TiO₂ nanoparticles was evaluated by measuring the decomposition rate of MB solution at room temperature. For comparison, the same measurements were also performed on the pure CSL and TiO₂. The temperature of the photocatalytic reaction was maintained at room temperature. The visible light was obtained from a 300 W Xe lamp (PLS-SXE300, Beijing Trusttech Co. Ltd.) with a UVCUT400 model filter (transparent for $\lambda > 400$ nm). For a typical photocatalytic experiment, a total of 0.06 g sample was added to 100 mL MB aqueous solution (5.0×10^{-4} mol/L) in a custom-made quartz reactor. The concentration of MB was monitored by UV–vis spectroscopy with maximum absorption at ~660 nm during the entire experiment. After 5 min or 10 min intervals during visible light illumination, about 3 mL aliquots were taken out and centrifuged to remove the trace particles. The absorbance of the centrifuged solution was measured in the range 500–800 nm using a UV–vis spectrophotometer (Shimadzu UV-2550). To determine the extent of mineralization during photocatalysis, total organic carbon (TOC) of centrifuged suspension samples were measured via a Shimadzu TOC-VCSH analyzer equipped with a Shimadzu ASI-V auto sampler device.

3. Results and Discussion

3.1 Characterization of samples

XRD and Raman spectroscopy were used to investigate the changes of structure and crystallite sizes of the CSL-modified TiO₂ nanoparticles obtained at different CSL amounts. Fig.1 (a) shows the XRD patterns of the samples obtained at various CSL amounts. All samples showed an anatase TiO₂ phase, indicating that the crystallization of the samples is achieved and that only anatase phase can be obtained. Moreover, CSL-modified TiO₂ nanoparticles do not cause any change in peak positions compared with pure TiO₂. However, the intensity of the main peak of modified catalyst is slightly lower than that of pure TiO₂, which shows that the addition of CSL affect the size of the TiO₂ nanoparticles. The Raman spectroscopy results of pure TiO₂ and CSL-modified TiO₂ nanoparticles indicated the decrease in the average size and crystallization of the as-prepared CSL-modified TiO₂ nanoparticles (experimental results are shown in the ESI, Fig. S1).

The average crystallite sizes of pure TiO₂ and CSL-modified TiO₂ nanoparticles were determined from the anatase peak (101) by using the Debye-Sherrer formula given by:

$$d = \frac{K\lambda}{\beta \cos\theta} \quad (3.1)$$

where d is the particle sizes, λ is the wave length of the X-ray radiation (0.15406 nm), K is the shape coefficient ($K=0.94$), θ is the diffraction angle and β is the full width at half maximum (FWHM) of the selected diffraction peak. The average crystallite sizes of the samples are 20.6 nm, 8.3 nm and 6.2 nm for pure TiO₂, 0.5 wt% and 2.0 wt% CSL-modified TiO₂, respectively.

This trend is also in consistence with TEM observation.

The typical microstructure of the samples was characterized by TEM and the results are shown in Fig. 1(b), (c) and (d). The average particle size of pure TiO₂ is estimated to be 25 nm with a wide particle size distribution and the morphology of particles is irregular (Fig 1b). When CSL was used as modifier, the morphology and size of newly-formed particles changed, as shown in Fig. 1(c) and (d). With the increase of the CSL amount, the morphology of the particles grows regular and the size becomes smaller. This further illustrates that the addition of CSL can affect the morphology and particle size of TiO₂. The smaller of the particles size, the greater of the surface area, then the better of the photocatalytic performance.²² Light efficiency can also be enhanced due to the increased specific surface area and multiple scattering.²³ The specific surface area (S_A) of the samples were estimated by the formula given by:

$$S_A = \frac{6}{\rho d} \quad (3.2)$$

where d is the particle size and ρ is the density of the bulk TiO₂ ($\rho = 3.9 \text{ g}\cdot\text{cm}^{-3}$). The surface area are 74.7 m²/g, 185.4 m²/g and 248.1 m²/g, for pure TiO₂, 0.5 wt% and 2 wt% CSL-modified TiO₂ nanoparticles, respectively. The results are consistent with the test results by nitrogen adsorption-desorption isotherm measurements (experimental results are shown in the ESI, Fig. S2).

FT-IR spectra are used to identify the surface functional groups of the samples. Fig. 2 shows the FT-IR spectra of pure TiO₂, CSL and the CSL-modified TiO₂ nanoparticles in the wavenumbers range from 500 cm⁻¹ to 4000 cm⁻¹. The broad bands near 3452 cm⁻¹ and the sharp

band peaking at 1400 cm^{-1} appeared in all of the four spectra are respectively ascribed to the stretching and bending modes of the surface hydroxyl groups.²⁴ The bands at 1130 cm^{-1} and the broad absorption peak from 800 cm^{-1} to 500 cm^{-1} , with maximum absorption at 620 cm^{-1} , is ascribed to the asymmetric stretching, symmetric stretching, and the bending modes of Ti-O-Ti, respectively.²⁵ The peak observed at 1670 cm^{-1} is assigned to the deformation vibration for H-O-H bonds, which is normally recognized as an important factor affecting photocatalytic activity.²⁶

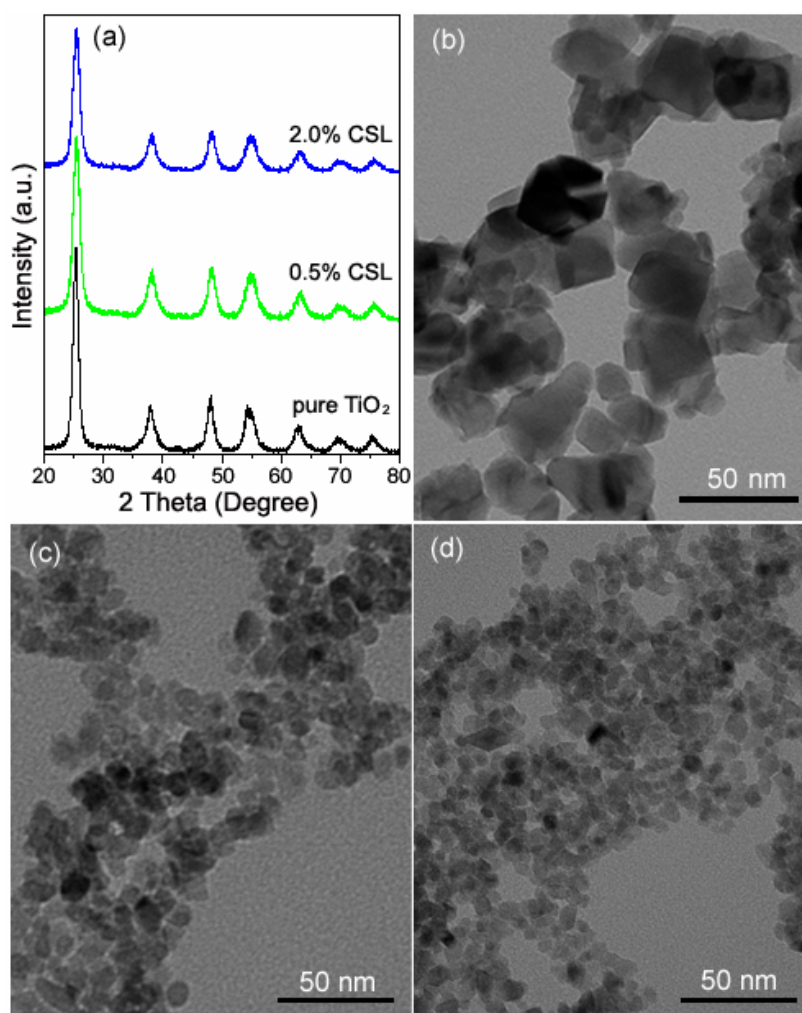


Fig. 1 (a): XRD patterns of pure TiO₂ and CSL-modified TiO₂ nanoparticles. (b), (c), (d): TEM

images of the pure TiO₂, 0.5 wt% and 2.0 wt% CSL-modified TiO₂, respectively.

The peak widths of the O-H stretching in CSL-modified samples are notably narrower than that of pure TiO₂. Typically, narrow peak indicates an enhanced intermolecular interaction among the functional groups. For example, narrow peak width of C-H stretch reflects greater packing density, thus leading to less mobility of alkyl chains in a self-assembled monolayer.²⁷ So, this phenomenon can also be applied to the interaction among surface hydroxyl groups. Since the surface hydroxyl groups play an important role in the photocatalytic process, with increase the amounts of surface hydroxyl groups by mixing with CSL, which can suppress electron-hole recombination and increase the photocatalytic efficiency.²⁸

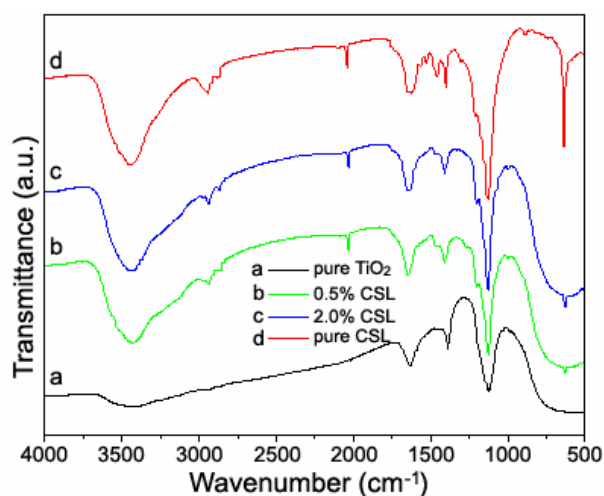


Fig. 2 FT-IR spectra of pure TiO₂, pure CSL, 0.5 wt% and 2.0 wt% CSL-modified TiO₂ nanoparticles.

As shown in Fig. 2, a few broad and weak absorption bands between 3000 cm⁻¹ and 1000 cm⁻¹ appear in our CSL-modified TiO₂ samples. Undoubtedly, the differences of the FT-IR spectra between the pure TiO₂ and CSL-modified TiO₂ samples are related to the introduction of

CSL source. The peaks from 2960 to 2850 cm^{-1} correspond to the C-H stretching mode of $-\text{CH}$, $-\text{CH}_2$ and $-\text{CH}_3$ bond.²⁹ The peaks observed at 1200 ~1180 cm^{-1} were characteristic of C-O asymmetric and symmetric vibrations. The peaks at 1650 ~1500 cm^{-1} are attributed to the C=C stretching vibration on the benzene ring, while the absorption peaks at 1450 to 1420 cm^{-1} were attributed to the in-of-plane bending vibration of C-H bonds. Bands at 1120 to 860 cm^{-1} were ascribed to the out-of-plane bending vibration of =C-H bond.³⁰

From the IR spectra, one can see that the pure CSL have two vibration peaks at about 870 cm^{-1} and 1445 cm^{-1} (Fig. 2d), which belong to the bending vibration of $-\text{OH}$ bond. The two peaks did not appear at the CSL-modified TiO_2 (Fig. 2b, c), suggesting that CSL was bound to the surface of TiO_2 via the carboxyl group and most likely the binding was a bidentate which was similar to other TiO_2 chelating agents such as ascorbic acid.²⁵

3.2 Optical properties and photocatalytic activity

CSL belongs to triterpenoids compound and contains resonance structure. The maximum absorption wavelength of it is 425 nm, which indicates that CSL shows strong absorption in visible light region. Hence, CSL may be as a photosensitizer for TiO_2 . Fig. 3a collects the UV-Vis diffuse reflectance spectra of the prepared CSL-modified TiO_2 , the pure TiO_2 and CSL. Inset is the photos of pure CSL and 0.5% CSL-modified TiO_2 samples. It is obvious that CSL has high absorption peak at about 425 nm. The strong absorption peak at 425 nm is caused by the $\pi \rightarrow \pi^*$ transition. In comparison to the pure TiO_2 , the spectra of the CSL-modified TiO_2 samples exhibit a stronger broad absorption band between 400–700 nm. The absorption intensity of CSL-modified TiO_2 samples in the visible light region increases with the increase of the CSL

amount. This further indicates that there is interaction between CSL and TiO_2 and our method is effective to extend the absorption of TiO_2 to visible light range. The absorption in the visible-light region implies that the prepared CSL-modified TiO_2 samples can be activated by visible light and that more electrons and holes can be photogenerated and participated in the desired photocatalytic reactions.

MB is a brightly colored blue cationic thiazine dye and is often used as a test model pollutant in semiconductor photocatalysis. Fig. 3b shows the photodegradation ability on MB solutions of pure TiO_2 , CSL and CSL-modified TiO_2 nanoparticles. The results show that under the illumination of visible light, the MB solutions containing the CSL-modified TiO_2 samples underwent significant degradation and became nearly transparent within 40 min. It should be noted that the 2.0 % CSL-modified TiO_2 sample exhibits the best photocatalytic activity. In contrast, pure TiO_2 and CSL almost do not decompose MB under visible light irradiation.

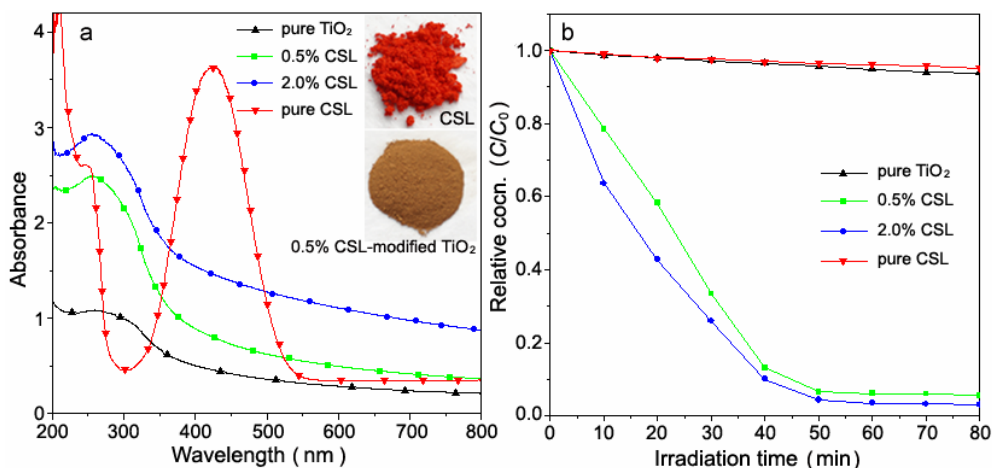


Fig. 3 (a) UV-vis spectra of pure TiO_2 , pure CSL, 0.5% and 2% CSL-modified TiO_2 nanoparticles. Inset is the photos of pure CSL and 0.5% CSL-modified TiO_2 samples. (b) Photodegradation of MB aqueous solutions by using pure TiO_2 , pure CSL and CSL-modified

TiO₂ samples as photocatalysts under visible light irradiation in neutral suspension.

The photocatalytic activity of the powders can be quantitatively evaluated by comparing their apparent reaction rate constants. Most of the photocatalytic oxidation of organic pollutants in aqueous suspensions follows the classical Langmuir–Hinshelwood kinetic model,³¹ the photocatalytic process of MB can be expressed as the following apparent pseudo-first-order kinetics equation:³²

$$\ln\left(\frac{C_0}{C_t}\right) = k_{app} \times t \quad (3.3)$$

where C_t is the concentration of aqueous MB at reaction time t , C_0 is the initial MB concentration, k_{app} is the apparent pseudo-first-order rate constant, and t is the reaction time. According to the experimental results, the variations in $\ln(C_0/C)$ as a function of the irradiation time are given in Fig. 4a. All the curves can be fitted roughly to a straight line. Thus, the photocatalytic degradation reaction is assumed to follow first-order kinetics. The rate constants of the 0.5 wt%, 2 wt% CSL-modified TiO₂ and pure TiO₂ nanoparticles are 0.038, 0.056 and 0.0013, respectively. Its are 29.23 and 43.08 times higher than that of pure TiO₂. Therefore, the CSL-modified TiO₂ nanoparticles exhibit strong photocatalytic activity for MB decomposition under visible-light irradiation.

The stability of a photocatalyst is highly important for its application. The cyclic stability test under the same conditions, i.e, the initially concentration of MB is 5.0×10^{-4} mol/L, of 2wt% CSL-modified TiO₂ nanoparticles was also examined and shows excellent photocatalytic activity in degrading MB solution, as shown in Fig. 4(b). No significant decrease in its photocatalytic

oxidation activity is observed after being used 10 times, which makes it very promising for practical application.

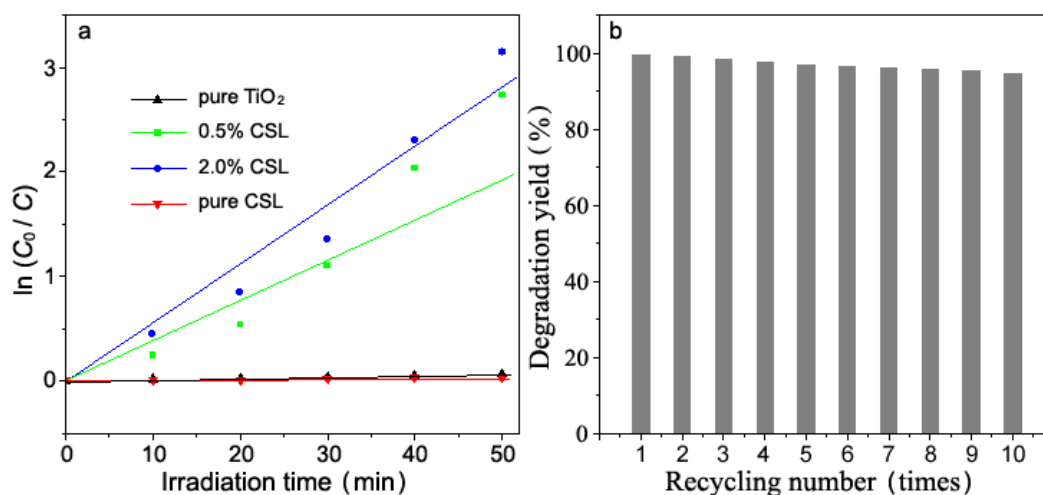


Fig. 4 (a) Variation in the normalized $\ln(C_0/C)$ as a function of visible-light irradiation time. (b) Recycling test result by using the 2wt% CSL-modified TiO_2 sample under the same conditions.

To eliminate the possibility that the enhanced photocatalytic activity of CSL-modified TiO_2 samples mainly results from their enhanced physisorption alone, the FTIR spectra of the 2wt% CSL-modified TiO_2 sample have been recorded before and after the photodegradation of MB. Fig. 5a is the IR result that mix MB and 2wt% CSL-modified TiO_2 sample and stirred in the dark for 30min, then centrifuged and drying. Fig. 5b is the IR result of 2 wt% CSL-modified TiO_2 nanoparticles after degradation. Comparative a and b shows that, in the dark with stirring, the MB molecules adsorption on the catalyst surface. After the photocatalytic reaction, the complicated vibrational modes of MB disappear (Fig. 5b). As illustrated in Fig. 5b and Fig. 2c, the FTIR spectra of pure 2wt% CSL-modified TiO_2 sample before (Fig. 2c) and after degradation (Fig. 5a) show no significant discrepancy. In contrast, the FTIR spectrum of MB (Fig. 5b) shows

more complicated vibrational modes due to the organic molecule. The distinct FTIR spectrum of CSL-modified TiO₂ nanoparticles before and after degradation and that of the pure methylene blue strongly suggests that the degradation is due to the photocatalytic degradation instead of any physisorption of methylene blue on the catalyst.

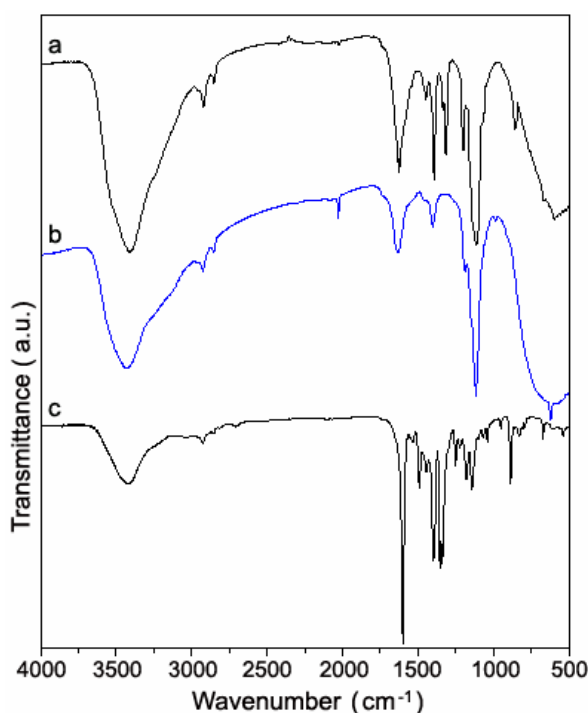


Fig. 5 FTIR spectra of (a) 2 wt% CSL-modified TiO₂ nanoparticles mix with MB before degradation, (b) 2 wt% CSL-modified TiO₂ nanoparticles mix with MB after degradation and (c) pure methylene blue.

Complete mineralization is very important for organic pollutants photocatalysis.³³ The decomposition of the MB molecule and subsequent mineralization leading to water and carbon dioxide could be visualized by the decrease in total organic carbon (TOC) during the photocatalytic process. To assess the extent of mineralization during the photocatalytic degradation of MB, TOC was monitored as shown in Fig. 6. It showed TOC decreases during

photocatalytic degradation of MB. Nearly 88% TOC removal was achieved after 70 min irradiation.

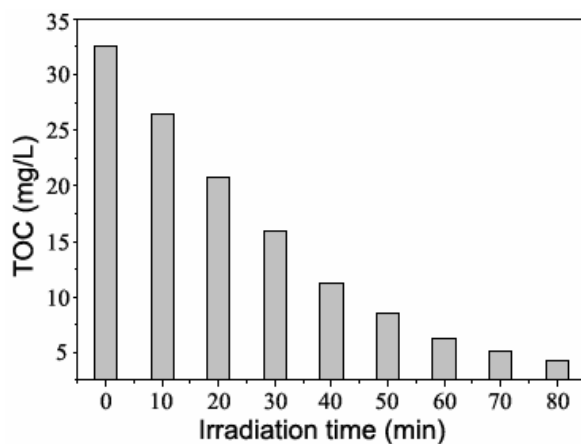


Fig. 6 Total organic carbon (TOC) removals during photocatalysis.

3.3 Proposed mechanism for the Enhanced Photocatalytic Activity

Generally, surface modifiers can affect the TiO_2 characteristics by three ways: (1) by inhibiting charge recombination; (2) by exploring the wavelength response range; (3) by changing the selectivity or yield of a particular product.³⁴ The PL emission has been widely used to explore the efficiency of charge carrier trapping, migration, and recombination in order to understand the fate of electron-hole pairs in semiconductor particles. The higher intensity of PL spectra reflects the higher rate of recombination.³⁵ Fig. 7a shows the room-temperature PL spectra for pure TiO_2 , CSL and CSL-modified TiO_2 samples excited by UV light at 380 nm. As shown in these spectra, the positions of the emission bands are similar and the PL intensity of the CSL-modified TiO_2 is relatively lower than that of pure TiO_2 . Since the PL emission is a result of recombination of excited electrons and holes, the lower PL intensity may indicate the lower recombination rate of electron–holes under the light irradiation.³⁶ The PL results indicate that the

photo-induced electron can transfer between CSL and TiO₂. When CSL is excited by light, the electron generated by the $\pi \rightarrow \pi^*$ transition can be transferred to the conduction band of TiO₂, and the electrons at the TiO₂ valence band can also be transferred to the CSL. This will effectively promote the separation of electronics-hole pairs, thereby enhancing the photocatalytic properties. In other words, the CSL-modified TiO₂ suppresses the recombination process, leading to a weak recombination of the electron-hole pairs and a high photocatalytic activity. However, for excitation with visible light at 425 nm, the CSL-modified TiO₂ samples exhibit much better PL effect than pure TiO₂ (Fig. 7b). The weaker of PL in pure TiO₂ is due to the insufficient energy of the visible photons that is lower than the band gap of pure TiO₂. In contrast, for the CSL-modified TiO₂ samples, the CSL modification allows absorption in the visible region to produce photoelectrons and holes.

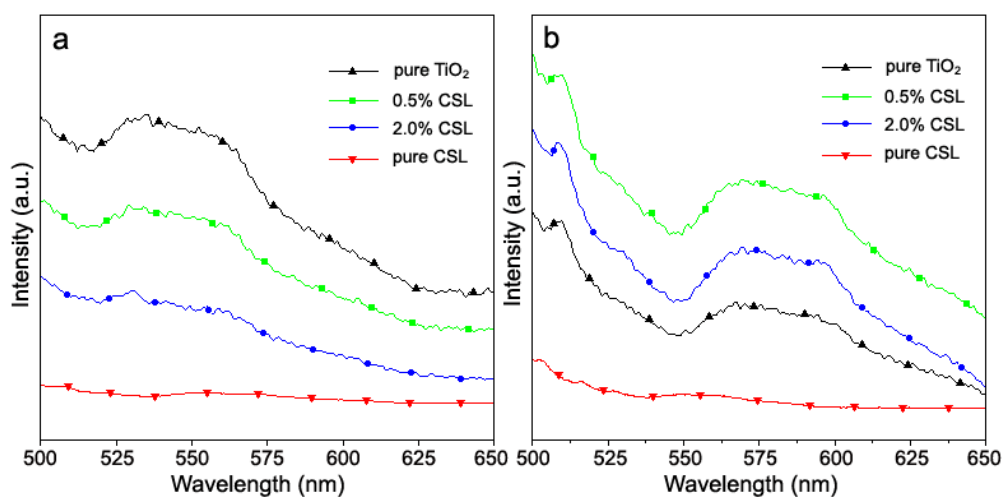


Fig. 7 PL spectra of pure TiO₂, CSL and the CSL-modified TiO₂ nanoparticles under UV-380 nm (a) and visible light 425 nm (b).

The effects of main active radical species (h^+ and $\bullet O_2^-$) suspected to be involved in the

photocatalytic process were investigated under visible light using a quantity of appropriate species quenchers (experimental results are shown in the ESI, Fig. S3). From the results, one can conclude that the $\bullet\text{O}_2^-$ radicals and h^+ almost played the same role for MB degradation. Based on the results of PL and photocatalytic tests, the photocatalytic mechanism under visible light irradiation can be suggested as follows. As shown in Fig. 8, when the CSL-modified TiO_2 nanoparticles are irradiated by using visible light, CSL absorbs visible light to induce electron transition. The excited-state electrons are transported from π -orbital to π^* -orbital. The excited-state electrons could be injected into the d-orbital (conductive band, CB) of TiO_2 readily and transferred to the nanoparticles surface to react with dissolved oxygen to generate superoxide radicals ($\bullet\text{O}_2^-$) (Fig. 8 (1)), which then become highly oxidative hydroxyl radicals ($\bullet\text{OH}$) through a series of oxidation reactions (Fig. 8 (2), (3)). At the same time, a positive charged hole (h^+) might be formed by electron migrating from TiO_2 valence band (VB) to CSL π -orbital, which can react with OH^- , H_2O or H_2O_2 to generate hydroxyl radicals ($\bullet\text{OH}$) (Fig. 8 (4)). The super-oxide radical ion $\bullet\text{O}_2^-$ and hydroxyl radical $\bullet\text{OH}$ are responsible for the degradation of organic compounds.^{8,30} Therefore, in contrast to bare TiO_2 nanoparticles, the higher photocatalytic activity of this system is due to the rapid charge separation and slow charge recombination. The superoxides attack MB and then completely photocatalyze oxidation cleavage of C=N, C=S, C-N and C-S bond. The smaller pieces are further completely oxidized to CO_2 , H_2O , NO_x^- and SO_4^{2-} by $\bullet\text{O}_2^-$, $\bullet\text{OH}$ or few $\bullet\text{HO}_2$ radicals (Fig. 8 (5)).

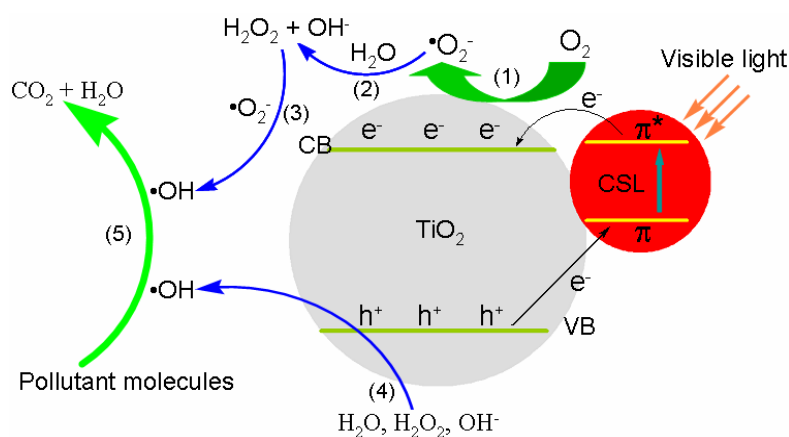


Fig. 8 The diagram of visible absorption and photocatalytic mechanism in the presence of CSL-modified TiO_2 nanoparticles.

4. Conclusion

In summary, celastrol (CSL), a triterpene derived from the Chinese medicinal plant *Tripterygium wilfordii*, was used to modify TiO_2 nanoparticles by the hydrothermal method. The resulting CSL-modified TiO_2 nanoparticles shows enhanced visible light-driven photocatalytic oxidation on MB. The high visible-light-driven photocatalytic activity of CSL-modified TiO_2 nanoparticles is ascribed to the synergetic effects of enhanced absorption of the CLS and increased efficiency in separation of photo-generated charge carriers. The as-prepared CSL-modified TiO_2 nanoparticles will show potential applications in various fields including photocatalysis, electrochemistry, biomedical field and so on. In addition, because the CSL have good biological activity and have been found to inhibit the proliferation of a variety of cancer cells and induce leukemic cell death, the introduction of CSL into the photosensitizer TiO_2 nanoparticles can optimize the use of Traditional Chinese medicine (TCM) and realize its

potential application for the multi-mode therapy of cancers. Further studies results will be summarized in our next study.

Acknowledgments

This work was supported by the Key Project of Natural Science Foundation of Shandong Province (ZR2013EMZ001), the Natural Science Foundation of Shandong Province (ZR2012BM021, ZR2011BQ01), the National Basic Research Program of China (973 Program, No. 2013CB632401) and the Project of Shandong Province Higher Educational Science and Technology Program (J10LF02, J12LA01, J11LB03).

References

- [1] a) A. Kubacka, M. Fernández-García, G. Colón, *Chem. Rev.*, 2012, **112**, 1555–1614; b) P. V. Kamat, *J. Phys. Chem. C*, 2012, **116**, 11849–11851.
- [2] a) A. Testino, I. R. Bellobono, V. Buscaglia, C. Canevali, M. D. Arienzo, S. Polizzi, R. Scotti, F. Morazzoni, *J. Am. Chem. Soc.*, 2007, **129**, 3564–3575; b) J. Zhang, Q. Xu, Z. C. Feng, M. J. Li, C. Li, *Angew. Chem. Int. Ed.*, 2008, **47**, 1766–1769.
- [3] a) B. Qi, Y. Yu, X. Q. He, L. Z. Wu, X. F. Duan, J. F. Zhi, *Mater. Chem. Phys.*, 2012, **135**, 549–553; b) P. Xu, T. Xu, J. Lu, S. M. Gao, N. S. Hosmane, B. B. Huang, Y. Dai, Y. B. Wang, *Energ. Environ. Sci.*, 2010, **3**, 1128–1134.
- [4] a) S. T. Kochuveedu, D. P. Kim, D. H. Kim, *J. Phys. Chem. C*, 2012, **116**, 2500–2506; b) H. Liu, X. Dong, G. Li, X. Su, Z. Zhu, *Appl. Surf. Sci.*, 2013, **271**, 276–283.

- [5] a) F. Zuo, K. Bozhilov, R. J. Dillon, L. Wang, P. Smith, X. Zhao, C. Bardeen, P. Y. Feng, *Angew. Chem.*, 2012, **124**, 6327–6330; b) M. Liu, X. Q. Qiu, M. Miyauchi, K. Hashimoto, *Chem. Mater.*, 2011, **23**, 5282–5286; c) X. Liu, L. R. Grabstanowicz, S. M. Gao, H. Xu, Z. Z. Lou, W. J. Wang, B. B. Huang, Y. Dai, T. Xu, *Nanoscale*, 2013, **5**, 1870-1875.
- [6] Y. C. Chen, Y. C. Pu, Y. J. Hsu, *J. Phys. Chem. C*, 2012, **116**, 2967–2975.
- [7] X. Li, W. H. Leng, *J. Phys. Chem. C*, 2013, **117**, 750–762.
- [8] J. H. Huang, M. A. Ibrahim, C. W. Chu, *RSC Adv.*, 2013, **3**, 26438-26442 .
- [9] X. H. Zhang, L. J. Yu, C. S. Zhuang, T. Y. Peng, R. J. Li, G. Li, *RSC Adv.*, 2013, **3**, 14363-14370.
- [10] Y. D. Tu, Z. Zhou, R. J. Yan, Y. P. Gan, W. Z. Huang, X. X. Weng, H. Huang, W. K. Zhang, X. Y. Tao, *RSC Adv.*, 2012, **2**, 10585-10591.
- [11] X. W. Li, R. G. Song, Y. Jiang, C. Wang, D. Jiang, *Appl. Surf. Sci.*, 2013, **276**, 761-768.
- [12] W. W. Zou, J. L. Zhang, F. Chen, *Mater Lett.*, 2010, **64**, 1710–1711.
- [13] K. Lv, J. C. Hu, X. H. Li, M. Li, *J. Mol. Catal. A: Chem.*, 2012, **356**, 78–84.
- [14] R. T. Thomas, N. Sandhyarani, *RSC Adv.*, 2013, **3**, 14080-14087.
- [15] J. G. Yu, L. Shi, *J. Mol. Catal. A: Chem.*, 2010, **326**, 8–14.
- [16] W. Y. Ahn, S. A. Sheeley, T. Rajh, D. M. Cropek, *Appl. Catal. B: Environ.*, 2007, **74**, 103–110.
- [17] H. L. Liu, Y. Zhou, H. Y. Huang, Y. Y. Feng, *Desalination*, 2011, **278**, 434–437.
- [18] D. F. Qiu, K. C. Liu, Z. J. Jiao, Q. Z. Huang, H. Z. Shi, M. Li, *Mater. Lett.*, 2013, **97**, 21–23.
- [19] a) S. Sreeramulu, S. L. Gande, M. Göbel, H. Schwalbe, *Angew. Chem. Inter. Ed.*, 2009, **48**,

- 5853–5855; b) H. R. Seo, W. D. Seo, B. J. Pyun, B. W. Lee, Y. B. Jin, K. H. Park, E. K. Seo, Y. J. Lee, Y. S. Lee, *Chemico-Biological Interactions*, 2011, **193**, 34–42.
- [20] H. Morita, Y. Hirasawa, A. Muto, T. Yoshida, S. Sekita, O. Shiota, *Bioorg. Med. Chem. Lett.*, 2008, **18**, 1050–1052.
- [21] J. Y. Li, X. M. Wang, H. Jiang, X. H. Lu, Y. D. Zhu, B. A. Chen, *Nanoscale*, 2011, **3**, 3115–3122.
- [22] a) X. J. Dai, Y. S. Luo, W. D. Zhang, S. Y. Fu, *Dalton Transactions*, 2010, **39**, 3426–3432; b) Z. Q. Tan, K. Sato, S. Takami, C. Numako, M. Umetsu, K. Soga, M. Nakayama, R. Sasaki, T. Tanaka, C. Ogino, A. Kondo, K. Yamamoto, T. Hashishin, S. Ohara, *RSC Adv.*, 2013, **3**, 19268–19271.
- [23] Z. L. He, W. X. Que, Y. C. He, *RSC Adv.*, 2014, **4**, 3332–3339.
- [24] K. Takahashi, H. Yui, *J. Phys. Chem. C*, 2009, **113**, 20322–20327.
- [25] C. Y. Song, W. J. Yu, B. Zhao, H. L. Zhang, C. J. Tang, K. Q. Sun, X. C. Wu, L. Dong, Y. Chen, *Catal. Commun.*, 2009, **10**, 650–654.
- [26] D. A. Panayotov, J. T. Y. Jr, *Chem. Phys. Lett.*, 2005, **410**, 11–17.
- [27] R. Varadaraj, H. Schaffer, J. Bock, Jr P. Valint, *Langmuir*, 1990, **6**, 1372–1376.
- [28] Y. Huang, W. K. Ho, S. C. Lee, L. Z. Zhang, G. S. Li, J. C. Yu, *Langmuir*, 2008, **24**, 3510–3516.
- [29] X. Y. Li, Z. R. Zhu, Q. D. Zhao, S. M. Liu, *Appl. Surf. Sci.*, 2011, **257**, 4709–4714.
- [30] Y. Ou, J. D. Lin, H. M. Zou, D. W. Liao, *J. Mol. Catal. A: Chem.*, 2005, **241**, 59–64.
- [31] C. Wu, H. Chang, J. Chen, *J. Hazard. Mater.*, 2006, **137**, 336–343.

- [32] J. G. Yu, G. H. Wang, B. Cheng, M. H. Zhou, *Appl. Catal. B: Environ.*, 2007, **69**, 171–180.
- [33] a) J. M. Hermann, *Catal. Today*, 1999, **53**, 115-129; b) S. Parra, V. Sarria, S. Malato, P. Peringer, C. Pulgarin, *Appl. Catal. B: Environ.*, 2000, **27**, 153-168.
- [34] A. P. Xagas, M. C. Bernard, A. H. L. Goff, N. Spyrellis, Z. Loizos, P. Falaras, *J. Photochem. Photobiol. A: Chem.*, 2000, **132**, 115–120.
- [35] H. F. Cheng, B. B. Huang, Y. Dai, X. Y. Qin, X. Y. Zhang, *Langmuir*, 2010, **26**, 6618–6624.
- [36] C. D. Valentin, G. Pacchioni, A. Selloni, *Chem. Mater.*, 2005, **17**, 6656–6665.